

Collisions of anisotropic two-dimensional bright solitons in dipolar Bose-Einstein condensates

Rüdiger Eichler,^{*} Damir Zajec,[†] Patrick Köberle, Jörg Main, and Günter Wunner
Institut für Theoretische Physik 1, Universität Stuttgart, 70550 Stuttgart, Germany
 (Dated: August 20, 2018)

We investigate the coherent collision of anisotropic quasi-two-dimensional bright solitons in dipolar Bose-Einstein condensates. Our analysis is based on the extended Gross-Pitaevskii equation, and we use the split-operator method for the grid calculations and the time-dependent variational principle with an ansatz of coupled Gaussian functions to calculate the time evolution of the ground state. We compare the results of both approaches for collisions where initially the solitons are in the repelling side-by-side configuration and move towards each other with a specific momentum. We change the relative phases of the condensates, and introduce a total angular momentum by shifting the solitons in opposite direction along the polarization axis. Our calculations show that collisions result in breathing-mode-like excitations of the solitons.

PACS numbers: 03.75.-b, 05.45.-a, 67.85.-d, 34.50.-s

I. INTRODUCTION

Bose-Einstein condensates (BECs) of magnetic atoms have attracted much attention since their experimental realization with ^{52}Cr atoms [1]. Recently, the creation of condensates of ^{164}Dy [2] and ^{168}Er [3] atoms with much larger magnetic moments than ^{52}Cr have also been reported. Furthermore, there has been fast progress towards the condensation of polar molecules with electric dipole moments [4], where the dipole-dipole interaction (DDI) is even more dominant. A review of the physics of dipolar bosonic quantum gases has recently been given by Lahaye *et al.* [5]. The features of the DDI being a non-local long-ranged and anisotropic interaction give rise to a variety of new effects. One example is the creation of solitary waves, where in analogy to nonlinear optics the effects of dispersion and nonlinearity may cancel each other. This leads to a condensate with a shape constant in time. The experimental realization of one-dimensional solitons in self-attractive BECs of ^7Li atoms has been reported [6]. Tikhonenkov *et al.* have theoretically predicted 2D solitons [7] and Köberle *et al.* have proposed a realistic experimental setup for the creation of a 2D soliton [8]. An exciting aspect of multidimensional solitons is their anisotropic nature, based on the in-plane polarization of the dipoles of such solitons. 2D solitons have already been studied using a variational ansatz with a single Gaussian and with coupled Gaussian functions [9]. Adhikari *et al.* have recently investigated axially symmetric and vortex solitons on a one-dimensional optical lattice [10]. Note that in contrast to systems with harmonic traps, where the density distribution in the trap direction is an approximate Gaussian, systems in an optical lattice will have an exponential density distribution.

The collision of axially symmetric bright 2D solitons has been studied by Pedri *et al.* [11] and Adhikari *et al.* [10]. Pedri *et al.* investigated a system with dipoles aligned parallel to the harmonic trap, while Adhikari *et al.* used an optical lattice instead. In both cases, the sign of the DDI has to be inverted by fast rotation of the orientation of the dipoles [12]. The resulting interaction energy becomes $U_d(\mathbf{R}) = -\alpha(3\cos^2\vartheta - 1)/R^3$, where ϑ is the angle between the polarization axis and $\mathbf{R} = \mathbf{r} - \mathbf{r}'$. The factor α can continuously be changed from $-1/2$ to 1. This provides the possibility to change the dipolar interaction from attractive to repulsive.

In addition to the analysis of the collision of 2D solitons, Young *et al.* [13] have investigated the collision of one-dimensional bright and vortex solitons. The investigations in [7–9] concentrated on the creation and the stability of 2D solitons with respect to small perturbations. However, one important property of solitons is that their shape is constant in time even when they are moving. Therefore, the collision of two solitons is an adequate scenario for the investigation of soliton dynamics far beyond small excitations. The influence of the nonlinear contact interaction and the DDI are of particular interest in such calculations.

As mentioned above, the creation of a BEC of magnetic atoms has been realized with a variety of species. Our results are valid for all dipolar systems, but we will add the corresponding values for a system with 20 000 ^{52}Cr -atoms per soliton in parentheses.

At sufficiently low temperatures, the dynamics of a Bose-Einstein condensate can be described by the extended Gross-Pitaevskii equation (GPE) which in atomic units and with particle-number scaling [14] reads

^{*} ruediger.eichler@itp1.uni-stuttgart.de

[†] zajec@itp1.uni-stuttgart.de

(Both authors contributed equally to this work)

$$\begin{aligned}
H(t)\Psi(\mathbf{r}, t) &= (-\Delta + V_{\text{har}} + V_{\text{sc}} + V_{\text{d}}) \Psi(\mathbf{r}, t) \\
&= i\partial_t \Psi(\mathbf{r}, t), \quad (1) \\
\text{with } V_{\text{har}} &= \gamma_y^2 y^2, \quad V_{\text{sc}} = 8\pi a |\Psi(\mathbf{r}, t)|^2, \\
V_{\text{d}} &= \int d^3 r' \frac{1 - 3\cos^2 \vartheta}{|\mathbf{r} - \mathbf{r}'|^3} |\Psi(\mathbf{r}', t)|^2.
\end{aligned}$$

Here a is the scattering length and Ψ designates the mean-field wave function. The dipoles are polarized along the z -axis, so that ϑ is the angle between the z -axis and the vector $\mathbf{r} - \mathbf{r}'$. We choose the y -direction as the axis of confinement perpendicular to the polarization axis where $\gamma_y = 20000$ (420 Hz), while the condensate is free in x - and z -direction. All simulations deal with condensates of low densities, and only a small period of time in which the two condensates merge to one transient condensate with higher density. This means that we do not need to take a three-body-loss term [8] into account, as the resulting absorption images ($|\psi|^2$ integrated along the y -axis) would only be slightly affected. We checked this assumption for the calculation of the collision without difference in phase and without angular momentum which up to the time of $t = 0.06$ ($t = 0.001$ corresponds to 15 ms) resulted only in a loss of about 5.5% of the particles.

As has been shown in [9], solitons only exist in a certain range of values of the scattering length, which can be tuned by the use of Feshbach resonances [15]. For too large values, the condensate will disperse, while too small values lead to the collapse of the condensate. In the following the scattering length is chosen to be 0.14 ($12.7a_{\text{B}}$, where a_{B} is the Bohr radius).

II. NUMERICAL APPROACH

The main theoretical task for the grid calculations is how to apply the time evolution operator $U = e^{-iHt}$ on a state $|\psi\rangle$. For this, one splits U symmetrically by using the Baker-Campbell-Hausdorff formula [16]

$$\begin{aligned}
U(\Delta t) &= e^{-iH\Delta t} = e^{-i(T+V)\Delta t} \\
&\approx e^{-i\frac{1}{2}T\Delta t} e^{-iV\Delta t} e^{-i\frac{1}{2}T\Delta t}, \quad (2)
\end{aligned}$$

where $V = V_{\text{har}} + V_{\text{sc}} + V_{\text{d}}$. One projects the action of the approximated time evolution operator on the basis of the position operator and makes use of the possibility to insert $\int d\nu |\nu\rangle \langle \nu| = 1$:

$$\begin{aligned}
\psi(\mathbf{r}, t + \Delta t) &= \langle \mathbf{r} | U(\Delta t) | \psi \rangle \\
&= \int d^3 p' d^3 r' d^3 p \langle \mathbf{r} | e^{-i\frac{p'^2}{2}\Delta t} | \mathbf{p}' \rangle \\
&\quad \langle \mathbf{p}' | e^{-iV(\mathbf{r})\Delta t} | \mathbf{r}' \rangle \langle \mathbf{r}' | e^{-i\frac{p^2}{2}\Delta t} | \mathbf{p} \rangle \langle \mathbf{p} | \psi \rangle \\
&= \frac{1}{\sqrt{2\pi}^9} \int d^3 p' d^3 r' d^3 p e^{i\mathbf{r}\mathbf{p}'} e^{-i\frac{p'^2}{2}\Delta t} \\
&\quad e^{-i\mathbf{p}'\mathbf{r}'} e^{-iV(\mathbf{r}')\Delta t} e^{i\mathbf{r}'\mathbf{p}} e^{-i\frac{p^2}{2}\Delta t} \tilde{\psi}(\mathbf{p}). \quad (3)
\end{aligned}$$

The structure of (3) suggests the following algorithmic procedure:

- Fourier transform of $\psi(\mathbf{r})$ in order to obtain $\tilde{\psi}(\mathbf{p})$
- Multiply by $e^{-i\frac{p^2}{2}\Delta t}$
- Inverse Fourier transform to real space
- Multiply by $e^{-iV(\mathbf{r})\Delta t}$
- Fourier transform to momentum space
- Multiply by $e^{-i\frac{p'^2}{2}\Delta t}$
- Inverse Fourier transform to real space

The potential V consists of the harmonic potential, the scattering potential and the DDI potential. The scattering potential and the DDI potential have to be calculated at each time step. The latter can be evaluated by means of the convolution theorem, which results in two more Fourier transforms:

$$\Phi_{\text{dd}}(\mathbf{r}) = \frac{4\pi}{3} \mathcal{F}^{-1} \left\{ \left(\frac{3k_z^2}{k^2} - 1 \right) \mathcal{F}\{|\psi(\mathbf{r})|^2\} \right\}. \quad (4)$$

Here k and k_z denote the momentum and the momentum in z -direction, respectively. Altogether, we have to perform six Fourier transforms for each time step. Note that the first and last Fourier transforms described in the algorithmic procedure of the time evolution are only necessary if one is interested in physical quantities whose evaluation requires the wave function in real space.

For the simulations, the spatial domain was discretized with up to $512 \times 128 \times 512$ grid points. Since this scheme is numerically very demanding, it has been implemented for graphics processing units (GPUs) using CUDA, enabling a very high degree of parallelization. Using the Tesla C2070 improves the performance of our algorithm by a factor of about 80 for double precision in comparison to the corresponding C algorithm using the well known FFTW library for computing the discrete Fourier transform on a IBM System x3400 with a Quad-Core Intel Xeon Processor E5430 (2.66GHz 12MB L2 1333MHz 80w) and 4 x 4GB PC2-5300 CL5 ECC DDR2 Chipkill Low Power FBDIMM 667MHz.

To investigate the coherent collision of solitons we have applied the following procedure. The first step is the computation of the ground state of one condensate using the split-operator method with imaginary time evolution ($t = -i\tau$). Afterwards we double the size of the grid in the x -direction and place two solitons in the repelling side-by-side configuration. The distance between the condensates is chosen such that they do not feel the mutual dipole-dipole interaction. To introduce momentum in the system, we multiply the left hand-side of the wave function by a plane wave e^{ikx} (for the soliton moving to the right) and the right hand-side by e^{-ikx} (for the soliton moving to the left), respectively.

III. TIME-DEPENDENT VARIATIONAL ANSATZ

Variational calculations using coupled Gaussian wave packets (GWPs) have shown to be a full-fledged alternative to numerical grid calculations for the calculation of ground states of dipolar BECs [9, 17]. The applicability of such ansatzes to dynamical simulations is a challenging task. The decisive extension of the previous work [9, 17] is that additional translational and rotational degrees of freedom are included in the ansatz with coupled GWPs to describe the dynamics of the condensate wave function. For the convenience of the reader we shortly review the time-dependent variational principle (TDVP) in this section, and subsequently apply it to the ansatz of coupled GWPs. We make use of the TDVP in the formulation of McLachlan [18] where ϕ is varied such that

$$I = ||i\dot{\phi} - H\Psi(t)||^2 \stackrel{!}{=} \min, \quad (5)$$

and set $\phi \equiv \dot{\Psi}$ afterwards. The wave function Ψ is considered to be parametrized by the variational parameters $\Psi = \Psi(\mathbf{z}(t))$. The minimization of the quantity I in Eq. (5) leads to

$$\left\langle \frac{\partial \Psi}{\partial \mathbf{z}} \left| i\dot{\Psi} - H\Psi \right. \right\rangle = 0, \quad (6)$$

which can be written in the short form

$$K\dot{\mathbf{z}} = -i\mathbf{h}, \quad (7)$$

with the positive definite Hermitian matrix K . We use a linear superposition of N Gaussian wave packets (GWPs)

$$\begin{aligned} \Psi &= \sum_{k=1}^N e^{-((\mathbf{x}^T - \mathbf{q}^k)^T A^k (\mathbf{x} - \mathbf{q}^k) - i(\mathbf{p}^k)^T (\mathbf{x} - \mathbf{q}^k) + \gamma^k)} \\ &\equiv \sum_{k=1}^N g^k, \end{aligned} \quad (8)$$

as an ansatz for the wave function in Eq. (5). In general, A^k are 3×3 complex matrices (determining the

width and the orientation of the GWP), \mathbf{p}^k and \mathbf{q}^k are three-dimensional real vectors (representing momentum and center of the GWP) and γ^k are complex numbers (where the real part stands for the amplitude and the imaginary part for the phase of the GWP, respectively). In this work we will make use of the strong confinement in one direction perpendicular to the dipole axis and omit the translational and rotational degrees of freedom in y -direction

$$A_{y\sigma}^k = A_{\sigma y}^k = 0, \quad p_y^k = 0, \quad q_y^k = 0, \quad (9)$$

with $\sigma = x, z$. Inserting the ansatz Eq. (8) in Eq. (6), sorting the result by powers of \mathbf{x} and identifying these terms with the coefficients of a time-dependent effective harmonic potential

$$V_{\text{eff}}^k = v_0^k + \mathbf{v}_1^k \mathbf{x} + \mathbf{x} V_2^k \mathbf{x}, \quad (10)$$

yields the equations of motion (EOM) for the variational parameters

$$\dot{A}^k = -4i(A^k)^2 + iV_2^k, \quad (11a)$$

$$\dot{\mathbf{p}}^k = -\text{Re } \mathbf{v}_1^k - 2\text{Im } A^k (\mathbf{q}^k - 2\mathbf{p}^k) - 2\text{Re } V_2^k \mathbf{q}^k, \quad (11b)$$

$$\dot{\mathbf{q}}^k = 2\mathbf{p}^k + \frac{1}{2}(\text{Re } A^k)^{-1}(\text{Im } \mathbf{v}_1^k + 2\text{Im } V_2^k \mathbf{q}^k), \quad (11c)$$

$$\begin{aligned} \dot{\gamma}^k &= 2i \text{Tr } A^k - i\mathbf{q}^k V_2^k \mathbf{q}^k + 4\mathbf{p}^k A^k \mathbf{q}^k + i(\mathbf{p}^k)^2 \\ &\quad - i\mathbf{q}^k \mathbf{p}^k - i\mathbf{p}^k \mathbf{q}^k - 2\mathbf{q}^k A^k \mathbf{q}^k + iv_0^k. \end{aligned} \quad (11d)$$

If we write Eq. (7) explicitly for GWPs, the set of linear equations for $\dot{\mathbf{z}}$ can be rewritten to one for the vector \mathbf{v} containing the coefficients of V_{eff}^k

$$K\mathbf{v} = \mathbf{r}, \quad (12)$$

for details, see [19, 20]. With the transformation given in Appendix A the EOM can now be integrated with a standard algorithm such as Runge-Kutta, where Eq. (12) has to be solved at every time step. The right-hand side vector \mathbf{r} with the components

$$\mathbf{r}^l = \sum_{k=1}^N \langle g^l | x_\alpha^m x_\beta^n V(\mathbf{x}) | g^k \rangle, \quad (13)$$

where $l = 1, \dots, N$; $\alpha, \beta = 1, \dots, 3$; $0 \leq n + m \leq 2$, contains integrals of the potentials in the GPE. It is one of the most important advantages of the method that nearly all of these integrals can be calculated analytically. However, the dipolar integral $\langle \Psi | V_d | \Psi \rangle$ can only be calculated analytically for GWPs centered in the origin without the additional translational degrees of freedom introduced in the ansatz (8). The analytical and numerical treatment of the dipolar integral is presented in Appendix B.

The procedure for the calculations is as follows: At first the equations of motion (11) for one soliton are integrated in imaginary time, with the wave function being normalized after every time step. Afterwards every

GWP of the wave function is copied and the resulting two solitons are positioned in the same way as given in Sec. II. Then for each GWP a corresponding momentum $\mathbf{p}^k = \pm p_x^k \mathbf{e}_x$ is added. For this starting configuration the EOM are finally integrated in real time.

IV. RESULTS

In Fig. 1 three grid calculations of colliding solitons without angular momenta prepared in the way given above are shown. For no phase difference constructive interference occurs and the condensates merge and split up in two solitons again. Note that the condensates after the split-up ($t = 0.049$, $t = 0.001$ corresponds to 15 ms) have a larger spatial distribution than before ($t = 0.011$). This indicates that the transfer of kinetic energy to internal energy has excited the solitons. This might either induce the dispersal of the solitons or lead to breathing-mode-like oscillations. The column in the middle shows a simulation with a difference of $\phi = \pi/2$ in phase, resulting in a collision where the soliton on the right eventually has a lower amplitude than the one on the left, so that we do not have symmetric behavior anymore. The transfer of kinetic energy is not as large as for $\phi = 0$, resulting in only slightly larger condensates at $t = 0.049$. In the case of a collision with a difference of $\phi = \pi$ in phase we can see destructive interference (column on the right), the solitons effectively repel each other. The transfer of kinetic energy into internal energy is once again smaller, corresponding to a just slightly larger condensate at $t = 0.049$. The occurrence of the broken symmetry in x -direction can be understood if one considers that a difference in phase of $\phi = 0$ and $\phi = \pi$ yields a wave function which is an eigenfunction of the parity operator, in the sense of $\Pi_{\pm}\Psi(\mathbf{r}, t) = \pm\Psi(-\mathbf{r}, t)$. A difference of $\phi = \pi/2$ on the other hand does not result in an eigenfunction of the parity operator, thus yielding an asymmetric dynamic of the condensates.

In Fig. 2 we compare the results for grid calculations and the variational ansatz for simulations, where we shifted both condensates in opposite directions along the polarization axis in order to introduce angular momentum. Both approaches are in very good agreement with only slight differences, in particular for times where both condensates merge, and when comparing the extensions of the solitons at $t = 0.049$. It is remarkable that a total number of only six GWPs is sufficient to reproduce the structures of the grid calculations and give the correct result for the configuration at the end of all three simulations. The first case without a difference in phase (Fig. 2a) once again leads the solitons to merge and split up afterwards, while a transient eddy-like structure appears in the course of the collision. As in the case with no angular momentum, the solitons either seem to disperse, or a breathing-mode-like oscillation has been excited. The amount of kinetic energy which has been transferred is lower than in the former case, leading to

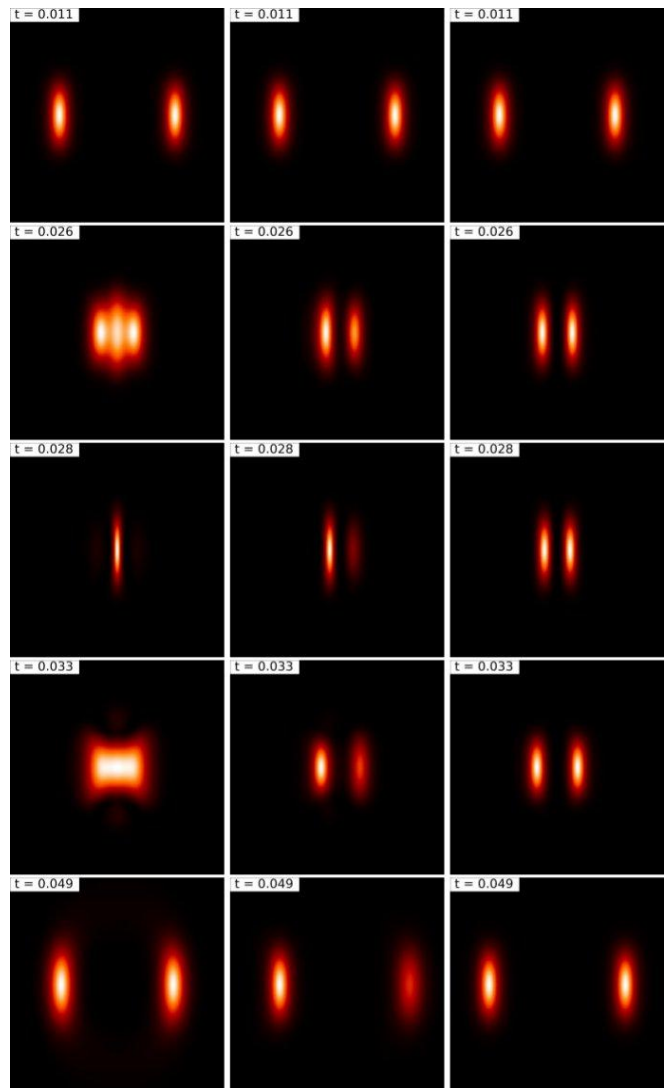


FIG. 1. (Color online) Absorption images ($|\psi|^2$ integrated along the y -axis) of grid calculations for the collision of solitons. The value of the momentum for each soliton is $k = 10$ (velocity $v = 127\mu\text{m/s}$) and the field of view is 1.4×1.4 ($135\mu\text{m} \times 135\mu\text{m}$). All absorption images have been normalized to the maximum value. Left column: Absorption images for a collision without difference in phase. Middle column: Absorption images for a collision with a difference of $\phi = \pi/2$ in phase. Right column: Absorption images for a collision with a difference of $\phi = \pi$ in phase.

condensates with smaller extension at $t = 0.049$ than their corresponding condensates in the simulation presented above. A difference of $\phi = \pi/2$ in phase (Fig. 2b) shows a similar behavior as in the case without angular momentum, resulting once again in an asymmetric situation where after the collision the condensates do not have the same amplitudes anymore. But for finite angular momentum one may actually speak of a merged condensate at $t = 0.031$. Finally the collision with a difference of $\phi = \pi$ (Fig. 2c) shows the condensates effectively repelling each other, but in this case introducing

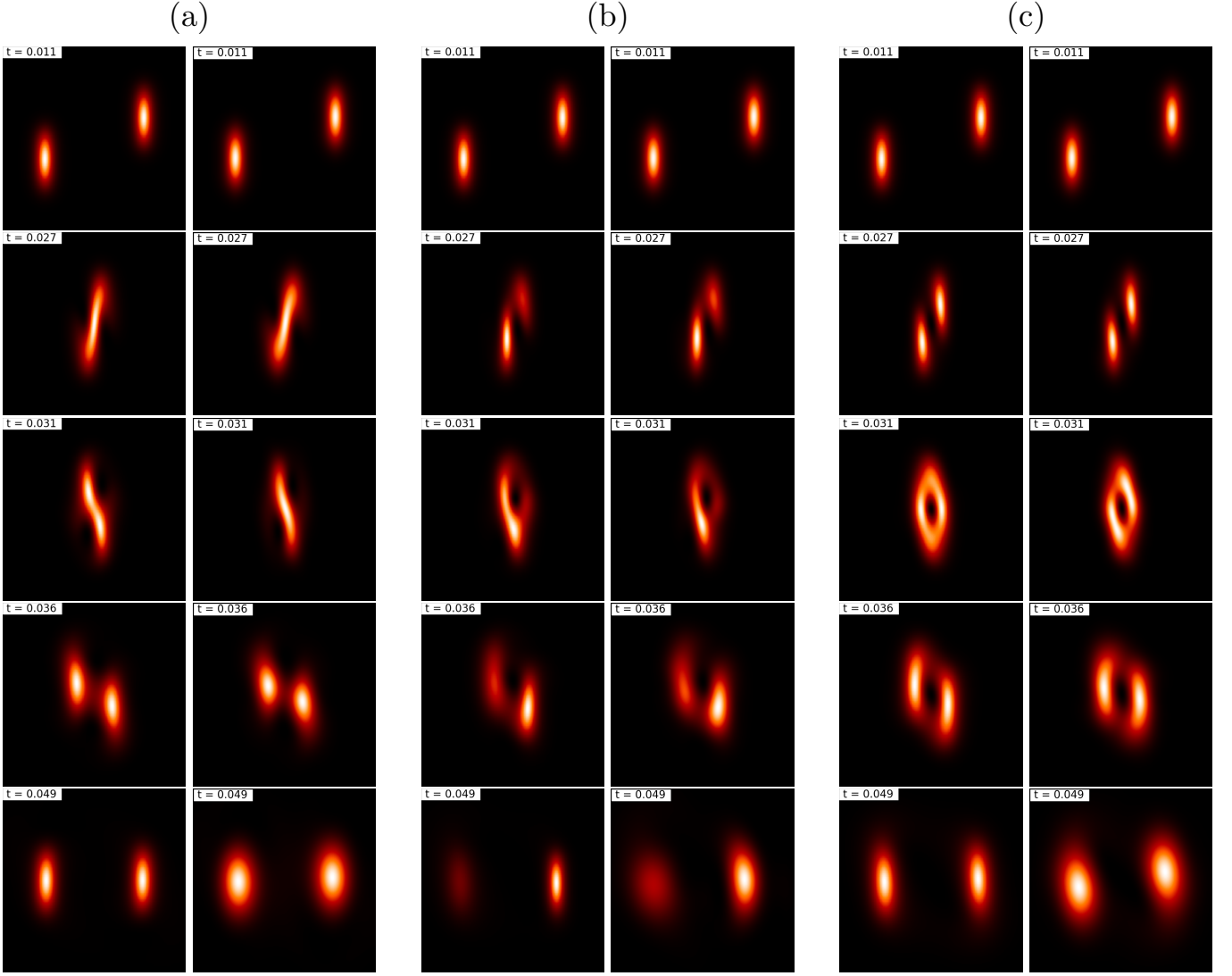


FIG. 2. (Color online) Absorption images for grid calculations and the variational ansatz of the simulation of two colliding solitons with angular momentum. All absorption images have been normalized to the maximum value. The parameters are the same as given in Fig. 1. The columns (a), (b) and (c) show calculations for a difference of $\phi = 0$, $\phi = \pi/2$ and $\phi = \pi$ in phase, where the left column is the result of the grid calculations and the column on the right hand-side presents the results of the variational ansatz. For all three calculations six GWPs (three for each soliton) were used. The variational calculation is able to reproduce the transient ring-like structure during the collision for a difference of $\phi = \pi$ in phase and yields the correct results for the configuration at the end of all three calculations.

angular momentum leads to a transient ring-like structure. The extension of the condensates after the collision is much larger compared to the case with no difference in phase, which means that the amount of transferred kinetic energy in internal energy is larger than in the former case. The case with angular momentum is suited best to show how the transfer of kinetic energy affects the spatial distribution of the condensate. In Fig. 3 we show the kinetic energy as a function of time for the collisions with angular momentum. Comparing the curves in Fig. 3 with the absorption images in Fig. 2, it is obvious that a larger transfer of kinetic energy implies a larger condensate at $t = 0.049$. The slightly smaller transfer observed

at the end of the full-numerical calculations (this leads to a larger extension of the solitons after the collision c.f. Fig. 2) originates from finite grid sizes and thus has no physical meaning. Variational calculations show an oscillation of the kinetic energy for large timescales, which corresponds to the excitation of the solitons.

The amount of kinetic energy transferred into internal energy of the solitons depends on the overlap of the wave functions during the collision process. A large overlap of the solitons enhances the nonlinear coupling in the GPE as $|\Psi(\mathbf{x}, t)|^2$ increases and a small one diminishes the coupling. This can be seen best in Fig. 1 (right column) where the destructive interference for the calcula-

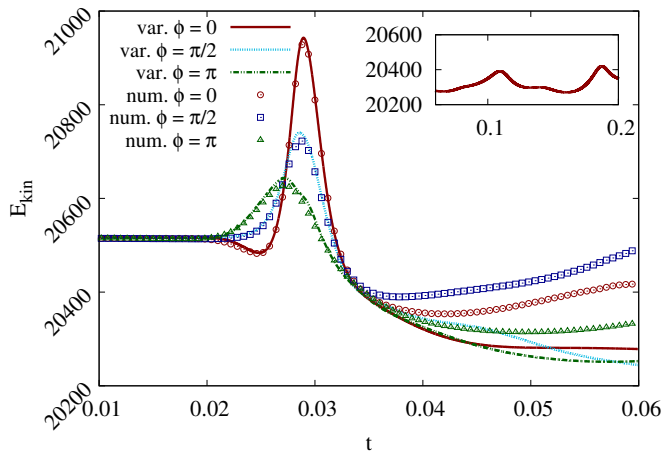


FIG. 3. (Color online) Kinetic energy as a function of time for the collisions with angular momentum (Fig. 2). The dots show the numerical results, the lines show the results obtained by the variational calculations. The kinetic energy increases while the condensates merge. After the split up, the condensates have a lower kinetic energy than before, indicative of a transfer from kinetic to internal energy, thus resulting in excitation of the condensates. The inset shows the kinetic energy obtained by the variational calculations for large timescales. The oscillatory behavior indicates the excitation of the solitons. Note the larger kinetic energy obtained by the grid calculations shortly after the split up. This is due to the finite grid size, which manifests itself in oscillations of the wave function's amplitude for large times.

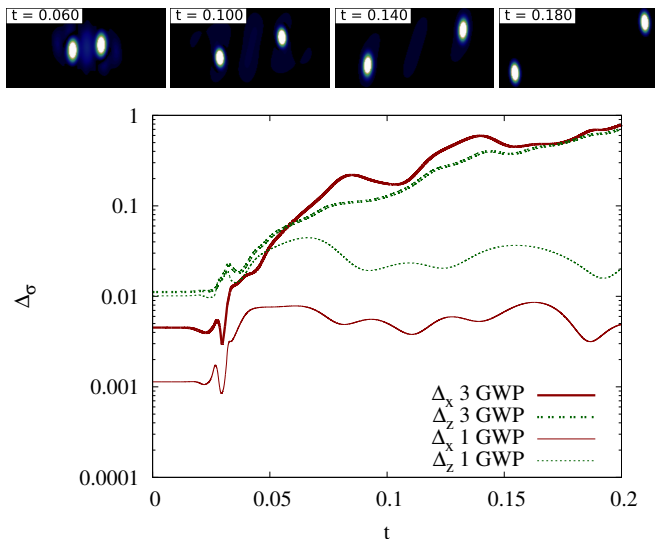


FIG. 4. (Color online) Variance Δ_σ of a single soliton (right soliton in the absorption images in the upper panel) as a function of time. The collision occurs at $t \approx 0.03$. The thick solid line and the double-dashed line show the Δ_x and Δ_z variance of three GWPs, respectively. The thin solid line and the normal dashed line show the Δ_x and Δ_z variance of the dominant GWP g^0 .

tion with phase difference $\phi = \pi$ leads to $|\Psi(\mathbf{0}, t)|^2 = 0$. For the corresponding calculation with nonzero angular momentum (Fig. 2c) we find $|\Psi(\mathbf{0}, t)|^2 = 0$, too. However, the ring-like structure increases the overlap during the collision.

In Fig. 4 the variance $\Delta_\sigma = \langle \sigma^2 \rangle - \langle \sigma \rangle^2$ with $\sigma = x, z$ is plotted as a function of time. The variance has been calculated for the three GWPs representing the solitons on the left-hand side in the starting configuration and for the GWP which has the largest amplitude after the collision process. This dominant GWP g^0 shows oscillatory behavior while the other GWPs with much smaller amplitudes describe particles leaving the soliton. This effect can hardly be seen in the absorption images in the upper panel of Fig. 4. However, the absorption images show that a soliton still exists, although this would be difficult to see in an actual experiment due to the very long time scale.

We have also performed simulations with smaller and larger momenta of the solitons. The former case leads to one merged condensate which does not split up again after the collision but shows oscillatory behavior. This is very similar to the collision presented in [11]. In the latter case the wavelength of the interference pattern is smaller and becomes more pronounced. Note that grid calculations with high momenta are problematic, because the condensates quickly reach the edge of the grid. An approach with a variational ansatz is better suited to analyze these scenarios.

V. CONCLUSION

We have studied the collisions of anisotropic two-dimensional bright solitons in dipolar Bose-Einstein condensates both with a fully-numerical ansatz and a time-dependent variational principle with coupled Gaussians. The calculations presented show that the collision process leads to an energy transfer from kinetic energy to “inner” energy of the solitons which leads to excited solitons with larger extent. The absorption images show very good qualitative agreement of the results gained by the two different methods.

The advantages of the grid calculations are the simplicity of the numerical scheme (although the implementation for the massively parallel computation requires some effort), the freedom in describing all different shapes of wave functions, and the numerical stability of the method. The advantages of the variational calculations are the much smaller numerical effort, enabling one to run long calculations on standard PCs, the independence of finite grid size, and the small amount of parameters to be saved.

Both methods can be used to simulate the time-dependent GPE, supporting each other mutually. One further application would be the inclusion of additional external potentials such as optical lattices and the comparison of the methods in such scenarios. Our results

should stimulate experimental efforts to study the collisions of 2D anisotropic solitons.

VI. ACKNOWLEDGEMENTS

We thank Boris Malomed for valuable discussions. This work was supported by Deutsche Forschungsgemeinschaft. R.E. is grateful for support from the Landesgraduiertenförderung of the Land Baden-Württemberg.

Appendix A: Transformation to CB -variables

The direct numerical integration of Eq. (11) leads to numerical difficulties [21]. These can be dealt with by the introduction of two auxiliary matrices B and C . With $A = BC^{-1}$ the equations of motion for the width matrices can be written as

$$\dot{A}^k = -4i(A^k)^2 + iV_2^k, \quad (A1)$$

$$\dot{A}^k = \dot{B}^k (C^k)^{-1} - B^k (C^k)^{-2} \dot{C}^k, \quad (A2)$$

where C and B are 3×3 complex matrices. Omitting the index k we obtain from these equations

$$B^{-1} \dot{B} C^{-1} - C^{-2} \dot{C} = -4iB^{-1}A^2 + iB^{-1}V_2 \quad (A3)$$

$$\Rightarrow B^{-1} \dot{B} - C^{-2} \dot{C} C = -4iC^{-1}B + iB^{-1}V_2 C. \quad (A4)$$

By comparison we yield the equations of motion for C and B

$$\dot{B}^k = iV_2^k C^k, \quad (A5)$$

$$\dot{C}^k = 4iB^k. \quad (A6)$$

The reduction (9) can be done for those matrices, too. Note however, that the matrices B and C do not preserve the same symmetry as the matrices A which are complex symmetric. Therefore, all five complex entries in B and C have to be integrated.

Appendix B: Solution of the dipolar integral

The calculation of the dipolar integrals needed in the TDVP $\langle \Psi | \alpha^n \beta^m V_d | \Psi \rangle$ with $\alpha, \beta = x, y, z$ and $0 \leq n + m \leq 2$ is shown here for the simplest case $n = m = 0$. The other integrals are calculated analogously. We start

from the six-dimensional non-local integral

$$\langle \Psi | V_d | \Psi \rangle = \sum_{l,k,j,i} \iint d^3r d^3r' g^{l*}(\mathbf{r}) g^{j*}(\mathbf{r}') g^i(\mathbf{r}') g^k(\mathbf{r}) \times \left(1 - \frac{3(z-z')^2}{|\mathbf{r} - \mathbf{r}'|^2} \right) \frac{1}{|\mathbf{r} - \mathbf{r}'|^3}. \quad (B1)$$

By the use of the convolution theorem of Fourier analysis we can evaluate one of the three-dimensional integrals directly, while the inverse Fourier transform

$$\langle \Psi | V_d | \Psi \rangle = \frac{1}{6\pi^2} \sum_{l,k,j,i} I_0^{kl} I_0^{ij} \times \int d^3k \exp \left\{ -\frac{1}{4} \mathbf{k}^T \bar{A}^{kl ij} \mathbf{k} + \frac{1}{2} i (\bar{\mathbf{p}}^{kl ij})^T \mathbf{k} \right\} \times \left(\frac{3k_z^2}{k^2} - 1 \right), \quad (B2)$$

remains to be done. Here I_0^{kl} denotes the overlap integral of the Gaussian functions k and l , and we have used the abbreviations

$$\bar{A}^{kl ij} = (A^{kl})^{-1} + (A^{ij})^{-1}, \quad (B3)$$

$$\bar{\mathbf{p}}^{kl ij} = (A^{ij})^{-1} \mathbf{p}^{ij} - (A^{kl})^{-1} \mathbf{p}^{kl}, \quad (B4)$$

with $A^{kl} = A^k + A^{l*}$ and $\mathbf{p}^{kl} = \mathbf{p}^k + \mathbf{p}^{l*}$ and analogously for i and j . The integral (B2) can be split in two parts, one leading to a shift in the scattering length (this is the short-range part of the DDI) and a second part $\langle \Psi | V_{d,\text{eff}} | \Psi \rangle = \sum_{l,k,j,i} I_0^{kl} I_0^{ij} J_2^{kl ij}$. After a principal component analysis of the exponential in Eq. (B2) the analytical integration in k_y -direction is possible when we make use of Eq. (9). The remaining result reads

$$J_2^{kl ij} = \frac{1}{4\pi} \int_0^\infty d\rho w \left(i \sqrt{\bar{A}_y^{kl ij} \frac{\rho}{2}} \right) \rho^2 e^{-\frac{1}{8} (\bar{A}_x^{kl ij} + \bar{A}_z^{kl ij}) \rho^2} \times \sum_{\substack{\pm x_c \\ \pm x_s}} \int_{-1}^1 dx \frac{(\pm c_1 x_c \pm c_0 x_s)^2}{\sqrt{1-x^2}} \times e^{-\frac{1}{8} (\bar{A}_x^{kl ij} - \bar{A}_z^{kl ij}) \rho^2 x + \frac{i}{2} (\pm \bar{p}_x^{kl ij} \rho x_c \pm \bar{p}_z^{kl ij} \rho x_s)}, \quad (B5)$$

with $x_c = \sqrt{(1+x)/2}$, $x_s = \sqrt{(1-x)/2}$, the coefficients c_0, c_1 of the rotation matrix from the principal component analysis and the Faddeeva function $w(z) = e^{-z^2} \text{erfc}(-iz)$. The numerical evaluation of this integral can efficiently be performed by a Taylor expansion of the Faddeeva function for which the single terms can be obtained by a recursion formula and using a Chebyshev quadrature for the x -integration. To improve the result we apply a Padé-approximation to the Taylor series.

The numerical integration of the dipolar integrals is the crucial part in this method. Dependent on the number of Gaussian functions N there is a total number of $C_{\text{num}} = (N^4 + N^2 - 2N)/4$ integrals to be calculated numerically and $C_{\text{elliptic}} = N(N+1)/2$ which can be expressed in terms of elliptic integrals.

-
- [1] A. Griesmaier, J. Werner, S. Hensler, J. Stuhler, and T. Pfau, Phys. Rev. Lett. **94**, 160401 (2005); Q. Beaufils, R. Chicireanu, T. Zanon, B. Laburthe-Tolra, E. Maréchal, L. Vernac, J.-C. Keller, and O. Gorceix, Phys. Rev. A **77**, 061601(R) (2008).
 - [2] M. Lu, S. H. Youn, and B. L. Lev, Phys. Rev. Lett. **104**, 063001 (2010); M. Lu, N. Q. Burdick, S. H. Youn, and B. L. Lev, Phys. Rev. Lett. **107**, 190401 (2011).
 - [3] K. Aikawa, A. Frisch, M. Mark, S. Baier, A. Rietzler, R. Grimm, and F. Ferlaino, Phys. Rev. Lett. **108**, 210401 (2012).
 - [4] K.-K. Ni, S. Ospelkaus, M. H. G. de Miranda, A. Pe'er, B. Neyenhuis, J. J. Zirbel, S. Kotochigova, P. S. Julienne, D. S. Jin, and J. Ye, Science **332**, 231 (2008).
 - [5] T. Lahaye, C. Menotti, L. Santos, M. Lewenstein, and T. Pfau, Rep. Progr. Phys. **72**, 126401 (2009).
 - [6] L. Khaykovich, F. Schreck, G. Ferrari, T. Bourdel, J. Cubizolles, L. D. Carr, and Y. Castin, Science **296**, 1290 (2002); K. E. Strecker, G. B. Partridge, A. G. Truscott, and R. G. Hulet, Nature **417**, 150 (2002).
 - [7] I. Tikhonov, B. A. Malomed, and A. Vardi, Phys. Rev. Lett. **100**, 090406 (2008).
 - [8] P. Köberle, D. Zajec, G. Wunner, and B. A. Malomed, Physical Review A **85**, 023630 (2012).
 - [9] R. Eichler, J. Main, and G. Wunner, Phys. Rev. A **83**, 053604 (2011).
 - [10] S. K. Adhikari and P. Muruganandam, J. Phys. B: At. Mol. Opt. Phys. **45**, 045301 (2012).
 - [11] P. Pedri and L. Santos, Phys. Rev. Lett. **95**, 200404 (2005).
 - [12] S. Giovanazzi, A. Görlitz, and T. Pfau, Phys. Rev. Lett. **89**, 130401 (2002).
 - [13] L. E. Young, P. Muruganandam, and S. K. Adhikari, J. Phys. B: At. Mol. Opt. Phys. **44**, 101001 (2011).
 - [14] P. Köberle, H. Cartarius, T. Fabčić, J. Main, and G. Wunner, New Journal of Physics **11**, 023017 (2009).
 - [15] C. Chin, R. Grimm, P. Julienne, and E. Tiesinga, Rev. Mod. Phys. **82**, 1225 (2010).
 - [16] M. D. Feit, J. A. Fleck, Jr., and A. Steiger, J. Comp. Phys. **47**, 412 (1982).
 - [17] S. Rau, J. Main, P. Köberle, and G. Wunner, Phys. Rev. A **81**, 031605(R) (2010).
 - [18] A. D. McLachlan, Mol. Phys. **8**, 39 (1964).
 - [19] S. Rau, J. Main, and G. Wunner, Phys. Rev. A **82**, 023610 (2010).
 - [20] S. Rau, J. Main, H. Cartarius, P. Köberle, and G. Wunner, Phys. Rev. A **82**, 023611 (2010).
 - [21] E. J. Heller, J. Chem. Phys. **65**, 4979 (1976).